A non-uniform multi-wideband OFDM system for Terahertz joint communication and sensing

A Non-Uniform Multi-Wideband OFDM System for Terahertz Joint Communication and Sensing

Yongzhi Wu[1], Filip Lemic[1,2], Chong Han[1], and Zhi Chen[3]
[1]Shanghai Jiao Tong University, China (email: {yongzhi.wu, chong.han}@sjtu.edu.cn)
[2]University of Antwerpen - imec, Belgium (email: filip.lemic@uantwerpen.be)
[3]University of Electronic Science and Technology of China, China (email: chenzhi@uestc.edu.cn)

***Abstract*—Recently researchers have been attracted by the joint communication and sensing (JCS) techniques, due to their diverse benefits in communication-sensing applications. By sharing the spectrum and hardware components, the advantages of JCS systems include enhanced spectrum efficiency and reduced device costs. Following the trend of scaling up the carrier frequencies for 5G and beyond, Terahertz (THz) band is envisioned as a promising chunk of spectrum featuring multi-GHz bandwidth windows. However, despite the great promise, the waveform design for THz JCS is still not explored enough. In this work, the design guidelines for THz JCS waveform are presented. With the help of these guidelines, a non-uniform multi-wideband orthogonal frequency division multiplexing (NMW-OFDM) THz system is proposed to overcome the limitations of OFDM based JCS. The proposed NMW-OFDM system is able to realize sub-millimeter-level accuracy of the range estimation by using a multi-stage sensing algorithm, which is three orders of magnitude improvement compared to the OFDM-based JCS system. In addition, the accuracy of velocity estimation can be enhanced by 10 times within a short frame time. Finally, the system can achieve unprecedented communication data rate of 100 Gbps without sacrificing the maximum detectable distance.**

I. Introduction

In recent years, with the exhaustion of spectrum resources in the microwave band and an increasing demand of wireless transmission with ultra-fast data rate and large density of connectivity, the adoption of higher spectrum is motivated. Following this trend of moving up the carrier frequencies, the Terahertz (THz) band (0.1-10 THz) is regarded as one of key chunks of spectrum in 5G and beyond communication systems. For example, new experimental licenses (95 GHz and 3 THz) have been recently opened up by the Federal Communication Commission (FCC) [1]. Owing to its ultra-broad bandwidth, the THz band has the potential to satisfy the requirements of the new generations of wireless communication systems.

In addition to communications with electromagnetic waves, the radio spectrum has also been widely used in the perception of the surrounding physical environment via sensing the echo of the transmitted signals reflected by objects [2]. Recently, attention has been drawn on joint communication and sensing (JCS) techniques, especially in the applications requiring dual-function of communication and sensing. Indoor JCS applications include wireless virtual/augmented reality (VR/AR) that implements ultra-fast data stream and posture recognition of human bodies. In outdoor scenarios, JCS techniques can be applied in automotive and unmanned aerial vehicles (UAVs). The employment of radar in these systems facilitates the detection of the targeted vehicles and contributes to the realization of autonomous/assisted driving, which performs better than light detection and ranging (LIDAR) or cameras at night. In this paper, we focus on THz joint communication and radar sensing, which estimates the range/velocity of the object by using the backscattered communication signals.

A popular approach to JCS is the multi-carrier waveform based on Orthogonal Frequency Division Multiplexing (OFDM) [3]–[6], which is also investigated in the millimeter wave (mmWave) band combined with multi-beam techniques using antenna arrays [7]. Furthermore, Orthogonal Time Frequency Space (OTFS) based JCS is proposed in [8] and shows higher data rate than OFDM, as well as robustness to Doppler effects, but introduces non-negligible cost in terms of receiver complexity. In addition, the spread spectrum single-carrier approach has also been studied in [3] and some radar-centric waveforms that cannot support high data rate are introduced in [9]. When it comes to THz frequencies, while the vehicular JCS in low THz bands is experimented with the time-sharing approach in [10], the THz JCS waveform design has not been investigated yet. With the hybrid beamforming and multiple-input-multiple-output (MIMO) techniques, THz OFDM is of great significance for THz communications over frequency selective channels [11]. However, the THz JCS based on OFDM is still an open issue due to the propagation peculiarities in the THz band [10].

In this paper, we propose a THz JCS framework using a tailored non-uniform multi-wideband OFDM (NMW-OFDM) waveform. To the best of our knowledge, our work is the first one to focus on THz joint communication and sensing waveform design. The distinctive contributions of this work are summarized as follows.

- We present the design guidelines for THz JCS, which demonstrate that the OFDM system with single configuration in one wideband cannot satisfy the requirements of THz JCS. **Motivated by these guidelines, we propose a novel NMW-OFDM system**, where multiple OFDM waveforms in each multi-wideband are produced with non-uniform subcarrier spacing parameters and then superposed. The proposed system is expected to take advantage of the long detectable distance from the small subcarrier spacing and the high sensing accuracy from the large subcarrier spacing.
- **We present a multi-stage sensing algorithm tailored for**

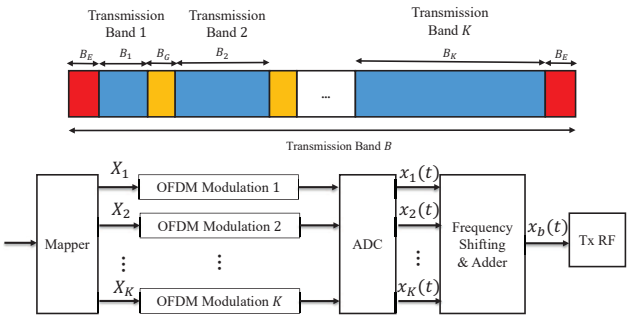

Fig. 1. Block diagram of the proposed NMW-OFDM system for THz JCS.

the NMW-OFDM THz system. This algorithm makes full use of the strengths of multiple sensing estimators with various detectable range and estimation accuracy, which estimate the target status from the received data frames in different subbands. Our simulations show that the proposed system, when utilizing the proposed algorithm, can realize sub-millimeter-level accuracy for range estimation, which is a three orders of magnitude improvement, compared to OFDM. In addition, the proposed system can achieve unprecedented data rate of 100 Gbps, which is significantly higher than that of the mmWave OFDM system.

The structure of this paper is organized as follows. The channel model and design guidelines for THz JCS are presented in Section II. In Section III, a novel NMW-OFDM THz system and a multi-stage sensing algorithm are proposed. In Section IV, the numerical results are carried out. Finally, the paper is concluded in Section V.

II. Channel Model and Design Guidelines for Terahertz JCS

A. Channel Model

Consider the radar return is reflected by P targets, whose distance away from the transmitter is r_p with the relative velocity v_p. The radar channel model is described by a multi-path time-variant impulse response

$$h_{\text{rad}}(t,\tau) = \sum_{p=1}^{P} \alpha_p e^{j2\pi\nu_p t}\delta(\tau-\tau_p) \tag{1}$$

where each target return corresponds to a reflected path with the path gain α_p, delay $\tau_p = \frac{2r_p}{c_0}$, and Doppler shift $\nu_p = \frac{2f_c v_p}{c_0}$. c_0 and f_c denote the speed of light and the carrier frequency, respectively. The path gain of the signal power is characterized by the THz channel model [12].

B. Design Guidelines

The range estimation in the frequency domain can be categorized as the following problem. Consider a sum of complex exponential signals buried in noise

$$z(n) = \sum_{p=1}^{P} A_p e^{j\varphi_p} e^{j2\pi n c\tau_p} + w(n) \quad n = 0,\cdots,N-1 \tag{2}$$

where the amplitude A_k and the phase φ_k are independent of A_l and φ_l if $k \neq l$, w is assumed to be additive white Gaussian noise (AWGN), $w \sim \mathcal{CN}(0,\sigma^2\mathbf{I})$, c is a constant. The problem is to estimate τ_p from $z(n)$. Evidently, if the real τ_p is not limited to some interval, the estimation result $\hat{\tau}_p$ can be estimated as the approximated values of $\tau_p + \frac{k}{c}(k \in \mathbb{Z})$. This implies that the estimation result is only non-ambiguous in the presence of the constraint $\frac{k_0}{c} \leqslant \tau_p < \frac{k_0+1}{c}$, where k_0 is some integer. Meanwhile, we can learn that the variance of $\hat{\tau}_p$ can be reduced by increasing the coefficient c.

In the range estimation, the coefficient c is determined by the subcarrier spacing Δf. Therefore, a feature of the OFDM based THz JCS is the periodicity of the radar range profile, which results in a maximum unambiguous range [4]

$$d_{\max} = \frac{c_0}{2\Delta f} \tag{3}$$

This is not a significant issue in the mmWave band, since the subcarrier spacing is small, and the maximum detectable distance is in the range of several hundreds of meters. In addition, the variance of the estimation error is proportional to $1/(\Delta f)^2$. From the above problem, we present the design guidelines for THz JCS here. If we want to make use of large bandwidth with OFDM radar in the THz band, it will become a challenge to maintain long maximum detectable range. It seems that the detectable distance and the sensing accuracy are contradictory for THz JCS. This feature guides us to consider a multi-wideband design, where some subbands with small subcarrier spacing are used to keep the ability of long detectable range and other subbands with large subcarrier spacing can improve the sensing accuracy and data rate, i.e., the subcarrier spacing in each subbands is non-uniform.

III. The Proposed NMW-OFDM System

In this section, we propose a non-uniform multi-wideband OFDM system and a multi-stage sensing algorithm to increase the maximum unambiguous range and the estimation accuracy for JCS in the THz band.

A. System Model

As is shown in Fig. 1, the sensing and communication modules share the common hardware from data source to transmitting antenna arrays at the transmitter end.

In the NMW-OFDM system, the total transmission band is divided into K subbands, whose parameters are independently configured with $\{B_i, \Delta f_i, T_0^{(i)}, T_{\text{cp}}^{(i)}, T_i, N_i, M_i\}, i = 1,2,\cdots,K$, where $B_i, \Delta f_i, T_0^{(i)}, T_{\text{cp}}^{(i)}, T_i, N_i, M_i$ refer to the bandwidth, subcarrier spacing, symbol duration, cyclic prefix, total symbol duration, number of subcarriers and number of symbols for one data frame in the i^{th} subband, respectively. Meanwhile, guard intervals B_G between adjacent subbands are reserved to reduce the inter-subband interference and guard bands B_E at both edges of the total transmission band are introduced to prevent out-of-band interference. Therefore, the whole bandwidth equals to the sum of the bandwidths of K subbands and the guard bands, $B = \sum_{i=1}^{K} B_i + 2B_E + (K-1)B_G$.

In the OFDM system, a transmitted OFDM data frame is denoted by $X[n,m] \in \mathcal{M}(n = 0,1,\cdots,N-1, m = 0,1,\cdots,M-1)$, where N and M are the number of sub-carriers and symbols in the transmitted frame, $\mathcal{M}$ is a modulation alphabet and determined by the modulation scheme, such as quadrature amplitude modulation (QAM) and phase shift keying (PSK). For instance, in 4-QAM modulation, the alphabet is given by $\mathcal{M} = \{\pm\frac{\sqrt{2}}{2} \pm \frac{\sqrt{2}}{2}j\}$.

In Fig. 1, the mapped information symbols form K data frames and the i^{th} data frame $X_i[n,m](n = 0,1,\cdots,N_i, m = 0,1,\cdots,M_i)$ is composed of N_i rows and M_i columns. Then X_i is modulated by the OFDM modulation with the parameter set of the i^{th} subband and generates a baseband signal,

$$x_i(t) = \sum_{m=0}^{M_i-1}\sum_{n=0}^{N_i-1} X_i[n,m]\left(\frac{t-mT_i}{T_i}\right) e^{j2\pi n\Delta f_i\left(t-T_{\text{cp}}^{(i)}-mT_i\right)} \tag{4}$$

where $X_i[n,m]$ denotes the symbol of X_i modulated on the n^{th} subcarrier at m^{th} time slot in the i^{th} subband, rect(t) is a rectangular pulse of unit duration and equals to 1 for $|t| \leq \frac{1}{2}$ and 0 for others. In the OFDM system, a cyclic prefix (CP) is introduced as a guard interval of duration $T_{\text{cp}}^{(i)}$. Therefore, the total duration of OFDM symbol T_i is the sum of original symbol duration $T_0^{(i)}$ and duration of CP $T_{\text{cp}}^{(i)}$, where $T_0^{(i)}$ has a relationship with the sub-carrier spacing, $T_0^{(i)} = \frac{1}{\Delta f_i}$.

To avoid the inter-symbol interference (ISI) and the inter-carrier interference (ICI), the subcarrier spacing Δf is required to satisfy $\nu_{\max} \ll \Delta f < B_{\text{c}}$, i.e., the subcarrier spacing should be much larger than the maximum Doppler shift $\nu_{\max}$ and lower than the coherence bandwidth B_c of the communication channel. For the radar detection, the delay spread between multiple targets should be smaller than $T_0^{(i)}$ and $T_{\text{cp}}^{(i)}$.

After OFDM modulations, The K baseband signals is shifted to the different subbands with the centering frequency $f_i = B_E + \sum_{k=1}^{i-1} B_i + (i-1)B_G + \frac{1}{2}B_i$ and then superposed as

$$x_b(t) = \sum_{i=1}^{K} x_i(t)e^{j2\pi f_i t} \tag{5}$$

The transmitted signal is reflected by P targets and produces the backscattered signal at the radar receiver. At the receiver side, the band-pass filter is used to obtain K baseband signals from the K subbands. The i^{th} baseband signal is demodulated by OFDM demodulation with the i^{th} parameter set. Totally, K received data frames $Y_i(i = 1,2,\cdots,K)$ are obtained to estimate the target distances. The i^{th} received data frame is

$$Y_i[n,m] = H_i[n,m]X_i[n,m] + W_i[n,m] \tag{6}$$

where $Y_i[n,m]$ refers to the symbol of Y_i demodulated from the n^{th} subcarrier at m^{th} time slot in the i^{th} subband, $H_i[n,m] = \sum_{p=1}^{P} \alpha_p e^{j\phi_p^{(i)}} e^{j2\pi\nu_p mT_i} e^{-j2\pi\tau_p n\Delta f_i}$ is essentially the frequency domain channel response, $\phi_p^{(i)}$ denotes the phase term that is independent of the subcarrier and symbol index, and $W_i[n,m]$ refers to the AWGN.

From the design guideline in Section II, we know that the range estimation through different received data frames can have different estimation accuracy and maximum ambiguous range, due to the use of multiple widebands with the configuration of non-uniform bandwidth and subcarrier spacing. Specifically, one subband with smaller subcarrier spacing can provide longer unambiguous range and another one with larger subcarrier spacing is able to achieve higher estimation accuracy. By combining them together, the overall system can take full advantage of their strengths.

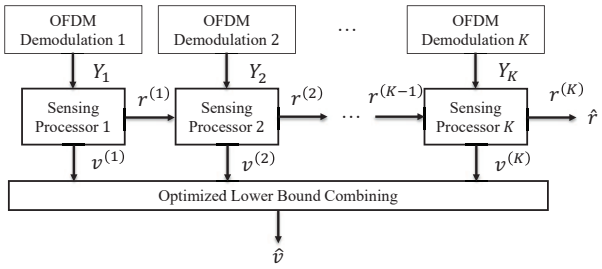

Fig. 2. The block diagram of the multi-stage sensing algorithm in the NMW-OFDM System.

B. Multi-Stage Sensing Algorithm

From each received frames in the NMW-OFDM system, we build K sensing processors with different unambiguous range and estimation accuracy, each of which obtains an estimated range and velocity of the target. Therefore, we propose a multi-stage sensing algorithm tailored for the NMW-OFDM system.

The block diagram of the multi-stage sensing algorithm is described in Fig. 2. We suppose that $\Delta f_1 < \Delta f_2 < \cdots < \Delta f_K$. First of all, K received data frames are demodulated from the OFDM demodulation with different parameter sets. For the first sensing processor, the received data frame Y_1 is used to estimate the targeted path distance r. Suppose that the maximum unambiguous range of the first sensing processor d_1 is equal to $d_{\max}$, which is longer than r, it has no ambiguity and outputs an estimated distance $r^{(1)}$. While the maximum unambiguous range of the second processor d_2 is likely to be smaller than the real targeted distance r, which causes the ambiguity of the range estimation, knowledge of $r^{(1)}$ from the first sensing processor is able to remove the ambiguity and helps the second one output an estimated value $r^{(2)}$,

$$r^{(2)} = \lfloor\frac{r^{(1)}}{d_2}\rfloor d_2 + r'^{(2)} \tag{7}$$

where $\lfloor\cdot\rfloor$ denotes the floor function and $r'^{(2)} < d_2$ refers to the ambiguous estimation of the second processor without knowing $r^{(1)}$. Then by cascading the K sensing processors and regarding the output of the previous processor as the input of the next one, the hierarchical sensing algorithm is implemented. The detailed procedure is stated in Algorithm 1.

The output of the multi-stage sensing algorithm is a linear combination of the estimated values from K sensing processors, which minimizes the estimation error. Next we describe how to select the weights of the sensing processors. In an AWGN channel, the Cramér-Rao lower bounds (CRLBs)

Algorithm 1: Multi-Stage Sensing Algorithm

Input: Received data frames: Y_i; Sensing processors: g_i; Maximum unambiguous range d_i; Weights of sensing processors: a_i, b_i $(i = 1, 2, \cdots, K)$

Output: Estimated range $\hat{r}$ and velocity $\hat{v}$

Initialization;

Find $(r^{(1)}, v^{(1)}) = g_1(Y_1)$, $r^{(1)} \in [0, d_1]$;

for $i = 2, \cdots, K$ **do**

  Find $(r'^{(i)}, v^{(i)}) = g_1(Y_1)$, $r'^{(i)} \in [0, d_i]$;

  Calculate $r^{(i)} = \lfloor \frac{r^{(i-1)}}{d_i} \rfloor d_i + r'^{(i)}$;

end

return $\hat{r} = \sum_{i=1}^{K} a_i r^{(i)}, \hat{v} = \sum_{i=1}^{K} b_i v^{(i)}$;

for the estimation variance using i^{th} estimator are given by $\text{Var}\left[r^{(i)}\right] = \frac{6}{\text{SNR}_i \cdot \left(N_i^2 - 1\right) N_i M_i} \left(\frac{c_0}{4\pi \Delta f_i}\right)^2$ and $\text{Var}\left[v^{(i)}\right] = \frac{6}{\text{SNR}_i \cdot \left(M_i^2 - 1\right) M_i N_i} \left(\frac{c_0}{4\pi T_i f_c}\right)^2$ [8], where SNR_i represents the signal-to-noise ratio (SNR) of the i^{th} received data frame. We formulate the *optimized lower bound combining (OLBC)* problem as

$$\begin{aligned} \min_{a_i, b_i} \quad & \text{Var}[\hat{r}] = \sum_{i=1}^{K} a_i^2 \text{Var}\left[r^{(i)}\right], \text{Var}[\hat{v}] = \sum_{i=1}^{K} b_i^2 \text{Var}\left[v^{(i)}\right] \\ \text{s.t.} \quad & \sum_{i=1}^{K} a_i = 1, \sum_{i=1}^{K} b_i = 1 \end{aligned} \tag{8}$$

When $\text{Var}[r^K] \ll \text{Var}[r^{(i)}] (i = 1, 2, \cdots, K-1)$, by using the method of Lagrange multipliers, we obtain

$$a_i \approx \begin{cases} 1 & , i = K \\ 0 & , i \neq K \end{cases}, b_i = \frac{\frac{1}{\text{Var}\left[v^{(i)}\right]}}{\sum_{i=1}^{K} \frac{1}{\text{Var}\left[v^{(i)}\right]}} \tag{9}$$

IV. Numerical Results

In this section, we provide the simulation results to illustrate the performance of the proposed NMW-OFDM system as compared with the OFDM system in the THz band. The carrier frequency f_c is set to 0.3 THz. We assume that the maximum subcarrier spacing Δf_{max} is 192 MHz, since the coherence bandwidth is considered to be less than 200 MHz. The OFDM frame time T_f is not over 5.34 μs, which contributes to low sensing latency and small symbol number. These values are taken in order to make all N_i and M_i exactly the exponents with the base of 2 when the maximum detectable distance equals to 100 m. We consider 32 subcarriers in range and velocity estimation to reduce the computational cost of the Monte-Carlo simulations. The reference target velocity is set to 20 m/s. We use the metric root mean square error (RMSE) to quantify the estimation accuracy of radar sensing.

A. Range Estimation

In Fig. 3, we show the curve of RMSE versus SNR in the range estimation, where the maximum detectable distance is 100 m and the range of the reference target is 60 m. Our results indicate that the RMSE of the NMW-OFDM system can achieve 10^{-4} m at low SNR and 10^{-5} m at high SNR, which is three orders of magnitude improvement compared to the OFDM system. According to the CRLB, the estimation error is inversely proportional to the subcarrier spacing and also can be reduced by increasing the symbol number with shorter symbol duration and fixed frame time. Therefore, the ultra-high accuracy of NMW-OFDM results from the large subcarrier spacing in the widest subband. Meanwhile, the waveform using the narrow subcarrier spacing in the first subband maintains the ability of a long unambiguous range detection. In addition, as visible in Fig. 3, the accuracy of NMW-OFDM with K = 3 is higher than the one obtained with K = 2 at SNR of -4 dB, while the latter becomes as large as the one achieved by the OFDM system. When the SNR is below a certain threshold, the error of the estimator g_1 employing the first subband may become large and obtain wrong estimated intervals for the remaining estimators in the multi-stage sensing algorithm. In this case, the accuracy of the proposed algorithm is the same as that the one achieved using only the first estimator, i.e., the accuracy of OFDM. By increasing the number of subbands, this SNR threshold can be reduced. In addition, we show the RMSE of a uniform multi-wideband OFDM (MW-OFDM) system with 10 subbands that have the same subcarrier spacing. While it can improve the range estimation accuracy by several times compared to the OFDM system, it is still much lower than that of NMW-OFDM system, since the use of non-uniform subcarrier spacing can provide the ultra-high accuracy.

In Fig. 4, different mappers are compared for the maximum detectable distance set to 12.5 m. The simulation results indicate that the RMSE of range estimation is increased when using higher-order QAM mappers. In order to conduct radar sensing, we first need to calculate the element-wise result of received data frames divided by the transmitting data frames. Under the 16-QAM modulation, the noise component is divided by different magnitudes of symbols and has a larger variance, which reduces the estimation accuracy. By comparing Fig. 3 and Fig. 4, it can be derived that the gap in estimation accuracies between the OFDM and NMW-OFDM systems is reduced when relaxing the maximum detectable distance.

B. Velocity Estimation

In Fig. 5, we compare the RMSE of velocity estimation in the OFDM and NMW-OFDM systems as functions of SNR. The accuracy is improved by one order of magnitude with the NMW-OFDM system compared the OFDM system. According to the CRLB of velocity estimation, the estimation error becomes larger when shortening the symbol duration but is reduced by increasing the symbol number.

C. Achievable Rate

In Fig. 6, we investigate the achievable rate to show the advantage of NMW-OFDM system in the THz band. In the mmWave system, the bandwidth is 100 MHz and the cyclic prefix is 1/8 of the symbol duration. The subcarrier number

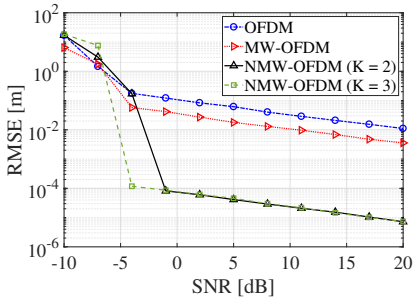

Fig. 3. RMSE versus SNR for range estimation in the OFDM, MW-OFDM and NMW-OFDM systems with the reference target distance of 60 m.

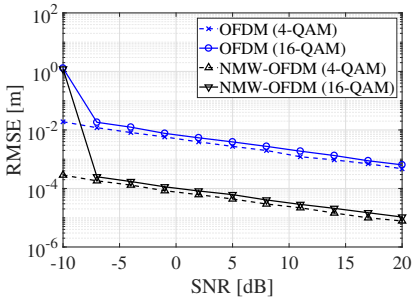

Fig. 4. RMSE versus SNR for range estimation using 4-QAM and 16-QAM with the reference target distance of 10 m.

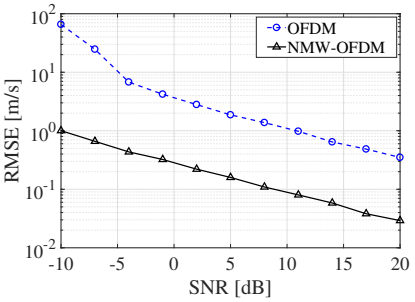

Fig. 5. RMSE versus SNR for velocity estimation in the OFDM and NMW-OFDM systems.

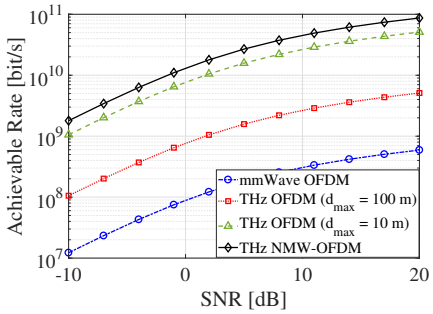

Fig. 6. Achievable rate versus SNR in the OFDM and NMW-OFDM systems.

and the available bandwidth of THz systems are usually lower than 1024 and 30 GHz, respectively.

As visible in Fig. 6, the achievable rate of the THz NMW-OFDM system is roughly 100 Gbps, which is significantly higher than the one achieved by the mmWave OFDM system. Due to the aforementioned limitation, the THz OFDM systems using the JCS waveform achieves a higher rate than the mmWave system, but lower than the NMW-OFDM system. Only by setting the maximum detectable distance to 10 m, the achievable rate of the THz OFDM system becomes comparable to the NMW-OFDM system.

V. Conclusions

In this paper, we present a NMW-OFDM framework to overcome the limitation of OFDM-based JCS system in the THz band. We provide a novel multi-stage sensing algorithm to make use of data frames from different subbands. We demonstrate that the proposed THz NMW-OFDM system is able to maintain a long detectable distance and realize a sub-millimeter-level accuracy of range estimation.

Our work shows that the range estimation accuracy in the NMW-OFDM system can be improved by three orders of magnitude compared to the OFDM system without reducing the maximum detectable range. Moreover, the accuracy of velocity estimation is improved by a order of magnitude in the case of short frame time. Finally, the NMW-OFDM THz system can achieve ultra-high data rate up to 100 Gbps, which is more than 100 times higher than the one attainable by the mmWave systems. Our future work includes investigating the effect of the weather conditions on the THz JCS.

Acknowledgment

Chong Han acknowledges the support from the National Natural Science Foundation of China (NSFC) under Grant 62027806. Filip Lemic acknowledges the support from the European Commission (EU MSCA-IF-2019, nr. 893760) and Research Foundation - Flanders (FWO, nr. V406320N).

References

[1] F. C. Commission, "FCC takes steps to open spectrum horizons for new services and technologies." [Online]. Available: https://docs.fcc.gov/public/attachments/DOC-356588A1.pdf

[2] M. Alloulah *et al.*, "Future millimeter-wave indoor systems: A blueprint for joint communication and sensing," *Computer*, vol. 52, no. 7, pp. 16–24, 2019.

[3] C. Sturm *et al.*, "Waveform design and signal processing aspects for fusion of wireless communications and radar sensing," *Proc. IEEE*, vol. 99, no. 7, pp. 1236–1259, July 2011.

[4] M. Braun *et al.*, "Co-channel interference limitations of ofdm communication-radar networks," *EURASIP Journal on Wireless Communications and Networking*, vol. 2013, no. 1, p. 207, August 2013.

[5] N. Nartasilpa *et al.*, "Communications system performance and design in the presence of radar interference," *IEEE Trans. Commun.*, vol. 66, no. 9, pp. 4170–4185, 2018.

[6] K. V. Mishra *et al.*, "Toward millimeter-wave joint radar communications: A signal processing perspective," *IEEE Signal Process. Mag.*, vol. 36, no. 5, pp. 100–114, 2019.

[7] J. A. Zhang *et al.*, "Multibeam for joint communication and radar sensing using steerable analog antenna arrays," *IEEE Trans. Veh. Technol.*, vol. 68, no. 1, pp. 671–685, January 2019.

[8] L. Gaudio *et al.*, "Performance analysis of joint radar and communication using ofdm and otfs," in *Proc. of IEEE ICC Workshops*, May 2019.

[9] S. M. Patole *et al.*, "Automotive radars: A review of signal processing techniques," *IEEE Signal Process. Mag.*, vol. 34, no. 2, pp. 22–35, March 2017.

[10] V. Petrov *et al.*, "On unified vehicular communications and radar sensing in millimeter-wave and low terahertz bands," *IEEE Wireless Commun.*, vol. 26, no. 3, pp. 146–153, June 2019.

[11] H. Yuan *et al.*, "Hybrid beamforming for mimo-ofdm terahertz wireless systems over frequency selective channels," in *Proc. of IEEE GLOBECOM*, December 2018.

[12] C. Han *et al.*, "Multi-ray channel modeling and wideband characterization for wireless communications in the terahertz band," *IEEE Trans. Wireless Commun.*, vol. 14, no. 5, pp. 2402–2412, May 2015.